Production and Characterization of a Novel Bilayer Nanocomposite Scaffold Composed of Chitosan/Si-nHap and Zein/POSS Structures for Osteochondral Tissue Regeneration

Sedef Tamburaci,[†,∥] Berivan Cecen,[‡] Ozcan Ustun,[§] Bekir Ugur Ergur,[§] Hasan Havitcioglu,[‡] and Funda Tihminlioglu[*,∥]

[†]Graduate Program of Biotechnology and Bioengineering, Gulbahce Campus, İzmir Institute of Technology, Urla, İzmir 35430, Turkey
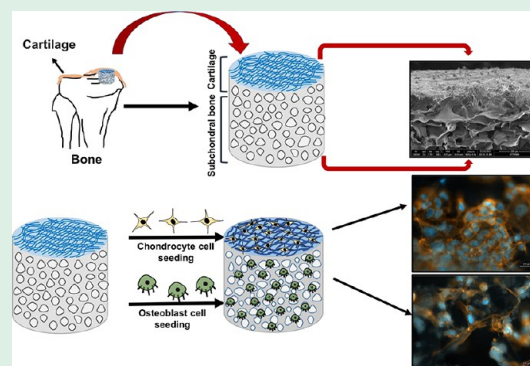
[‡]Department of Biomechanics, Institute of Health Science, Inciralti Health Campus, Dokuz Eylul University, İzmir 35220, Turkey

[§]Faculty of Medicine, Basic Medical Sciences, Histology and Embryology, Inciralti Health Campus, Dokuz Eylul University, İzmir 35220, Turkey

[∥]Department of Chemical Engineering, Gulbahce Campus, İzmir Institute of Technology, Urla, İzmir 35430, Turkey

ABSTRACT: Osteochondral tissue is hard to regenerate after injuries or degenerative diseases. Traditional treatments still have disadvantages, such as donor tissue availability, donor site morbidity, implant loss, and limited durability of prosthetics. Thus, recent studies have focused on tissue engineering strategies to regenerate osteochondral defects with different scaffold designs. Scaffolds have been developed from monolayer structures to bilayer scaffolds to repair the cartilage−bone interface and to support each tissue separately. In this study, Si-substituted nano-hydroxyapatite particles (Si-nHap) and silica-based POSS nanocages were used as reinforcements in different polymer layers to mimic a cartilage−bone tissue interface. Chitosan and zein, which are widely used biopolymers, are used as polymer layers to mimic the structure. This study reports the development of a bilayer scaffold produced via fabrication of two different nanocomposite layers with different polymer-inorganic composites in order to satisfy the complex and diverse regenerative requirements of osteochondral tissue. The chitosan/Si-nHap microporous layer and the zein/POSS nanofiber layer were designed to mimic a bone−cartilage tissue interface. Bilayer scaffolds were characterized with SEM, compression, swelling, and biodegradation tests to determine morphological, physical, and mechanical properties. The results showed that the bilayer scaffold had a structure composed of microporous and nanofiber layers joined at a continuous interface with appropriate mechanical properties. Furthermore, in vitro cell culture studies have been performed with LDH, proliferation, fluorescence imaging, and ALP activity assays using osteosarcoma and chondrosarcoma cell lines. ALP expression levels provide a good illustration of the improved osteogenic potential of a porous chitosan/Si-nHap layer due to the Si-doped nHap incorporation. Histological data showed that both fiber and porous layers that mimic the cartilage and bone sections exhibit homogeneous cell distribution and matrix formation. Histochemical staining was used to determine the cell proliferation and ECM formation on each layer. In vitro studies indicated that zein-POSS/chitosan/Si-nHap nanocomposite bilayer scaffolds showed promising results for osteochondral regeneration.

KEYWORDS: zein, osteochondral tissue, bilayer scaffold, chitosan, POSS

■ INTRODUCTION

The orthopedic tissue interfaces, which are responsible for the functional interactions between the adjoining tissues by reducing the formation of stress and resulting in the load bearing flexibility, are classified into three transition forms of hard to soft tissues as bone−cartilage, bone−tendon, and bone−ligament.[1] In bone−tissue interfaces, the physical characteristics of biomaterial are important to control the differences in structure and mechanical properties to mimic the hard and soft regions of the interface representing bone and connective tissue (cartilage), respectively. Therefore, different structures of bone and connective tissue obstruct the interface mimic by fabricating the biomaterial in monolayer form with conventional techniques.[2]

The osteochondral tissue is a multiphasic structure composed of two main parts: the articulating cartilage, which is responsible for reducing friction and absorbing shock in movement, and the subchondral bone, which is responsible for providing mechanical support. Articular cartilage is located at the end of joint surfaces and covers the articulating ends of the bones inside the

synovial joints. It has an important role in joints by forming a low friction contact interference and reducing the stress on the subchondral bone. It is composed of chondrocytes within a collagen fiber matrix, linked to glycosaminoglycan groups and elastin fibers.[3,4] Articular cartilage has a characteristically limited regeneration capacity. Thus, clinical treatments for osteochondral defects are autologous allogeneic cartilage tissue grafting and autologous chondrocyte implantation. However, problems associated with these approaches include calcification, restricted applications to focal lesions, shortage of donor—donor sites, the volume of donor tissue that can be safely harvested, donor site pain and morbidity, the possibility of harmful immune responses, transmission of disease, and rejection of grafts. Therefore, recent studies have focused on tissue engineering applications as an alternative to the traditional techniques.[5,6] The stability of cartilage tissue is bound up with subchondral bone and the interface between cartilage and bone. Thus, multilayered structures are needed to be used in scaffold design to provide the convenient support for each tissue separately and mimic the bone—cartilage tissue interfaces. Layered scaffold designs can mimic the osteochondral tissue which is composed of a gradual transition interface with regions showing different microstructure, mechanical properties, and chemical composition.[7,8] Studies have been focused on the use of natural polymers as scaffolds or biomaterials for tissue engineering applications. Nevertheless, these polymeric scaffolds still have major limitations such as insufficient mechanical properties and biological stability. Thus, natural polymers are generally chemically treated or reinforced with inorganic materials to enhance the mechanical properties and biological stability.[9]

Zein is a major storage protein of corn with a molecular structure composed of helical wheel confirmation with homologous repeating units arranged in an antiparallel form stabilized by hydrogen bonds. Zein protein is neither soluble in pure water nor in alcohol due to having both hydrophilic and hydrophobic characters. This leads to its solubility in aqueous solutions of ethanol (60—95% v/v).[10] Zein has been widely used as an edible packaging material in the form of a biodegradable film. Besides, it has been recently used as controlled drug delivery systems with its solubility, antioxidative, and antimicrobial activity.[9,11,12] Zein is an excellent protein for fiber matrix formation with the electrospinning technique due to its solubility in ethanol. However, its poor mechanical strength and morphological stability in aqueous environments are known as limitations and restricts. Zein fiber with its protein structure swells and collapses when interacted with water. Thus, zein is used with other polymers or cross-linking agents to improve the water stability in parallel with mechanical resistance.[13–15]

In bone tissue engineering applications, chitosan has been widely used due to its nontoxicity, nonallergenicity, structural similarity to glycosaminoglycans, biocompatibility and biodegradability, and ease of processability. Thus, chitosan is reinforced with inorganic fillers to mimic bone structure due to its stability problem and low mechanical strength.[16–18]

Silica nanoparticles have been widely used as reinforcements for biomedical applications.[19,20] Recent studies have focused on silica reinforcement for cartilage and bone tissue regeneration. Silica nanoparticles support bone cell adhesion and stimulate the osteogenic responses, inducing CaO deposition as well as providing enhancement in the structure by improving mechanical properties.[19,21,22] In addition, Si is found in high levels bound to extracellular matrix compounds and thus plays an important role in cartilage extracellular matrix formation.

Therefore, recent studies have focused on the inducing effect of silicate-based particles in both cartilage and bone regeneration.[23–26]

Among silica nanoparticles, polyhedral oligomeric silsesquioxanes (POSS) are known as the smallest ones (1.5 nm) with a well-defined cage structure and chemical composition, which contain an inorganic silicon/oxygen cage and organic hydrocarbon functional groups.[27] POSS incorporation can enhance thermal, rheological, and mechanical properties. In addition, different R groups of POSS nanocages provide a high compatibility with polymer systems.[28,29] POSS nanocages also influence the surface wettability and topography of the polymer matrix at a nanoscale. These alterations lead to improvement for cell attachment and differentiation.[29]

Recently, POSS nanocages have been used as drug delivery systems[30] and cardiovascular[31,32] and dental nanocomposites.[33,34] However, there are limited studies regarding the polymer/POSS nanocomposite designs for hard tissue regeneration.[18,35–37]

Recent developments for regeneration of a bone—cartilage interface have focused on gradient or layered scaffold designs to obtain structural integrity as well as mimicking both bone and cartilage. In this study, the aim was to fabricate novel bilayer scaffolds with a different morphology to mimic the osteochondral tissue. Si-doped nHap particles and novel POSS nanocages were used to enhance bioactivity of the scaffold as well as reinforce the structure. There are few studies regarding the promising properties of POSS nanocages for chondrogenic tissue formation. However, there are limited studies concerning the use of POSS nanocages with a natural polymer matrix as biomaterials for cartilage regeneration. Therefore, the aim of this study is to design novel bilayer biomaterials consisting of two different natural polymer composites as a cartilage—bone tissue interface.

■ EXPERIMENTAL SECTION

Materials. Chitosan (medium molecular weight) and zein (corn maize) (Sigma-Aldrich) were used in preparation of bilayer nanocomposites. Octa-TMA POSS (Hybrid Plastics TM) and nanohydroxyapatite (Si-nHap) (Sigma-Aldrich) were used for reinforcements. Acetic acid (analytical grade, Sigma -Aldrich) was used as a solvent for the preparation of nanocomposites. Minimum essential medium (MEM, Sigma-Aldrich), fetal bovine serum (FBS-Lonza), penicillin-streptomycin solution (03-033-1B Biological Industries), and L-glutamine (200 mM, G7513, Sigma-Aldirch) were used for cell culture studies. An LDH kit (Thermo Fisher Scientific) and resazurin assay (Cell signaling, 11884) were used to determine cell cytotoxicity and proliferation, respectively. A BCA kit (Thermo Fisher Scientific) was used to determine the total protein content. An ALP assay kit (Biomerieux, Enzyline PAL Optimise) was used to determine alkaline phosphatase activity. Paraformaldehyde (PFA, Merck) was used for cell fixation. DAPI (Cell Signaling Technology) and Alexa Fluor 455 (Thermo Fisher Scientific, Molecular Probes) were used for fluorescence staining. Mouse monoclonal anticollagen type 1 and type 2 (Sigma-Aldrich) were used for immunohistochemical analyses.

Preparation of the Chitosan/Si-nHap Porous Layer. The chitosan/Si-nHap nanocomposite was prepared by separately preparing 1% w/v medium molecular weight chitosan in acetic acid (1% v/v) solution and Si-nHap (10—40% w/w) dispersions. Si-nHap particles were dried overnight to prevent agglomeration before use. Then the polymer solution and Si-nHap dispersion were mixed followed by continuous stirring and sonication with a Misonix Ultrasonic Liquid Processor for 30 min at 15 °C and 35 Amplitude for homogenization. The mixture was poured into 48-well plates for molding, and the plates were kept at −20 °C for 24 h. Then, the frozen solutions were
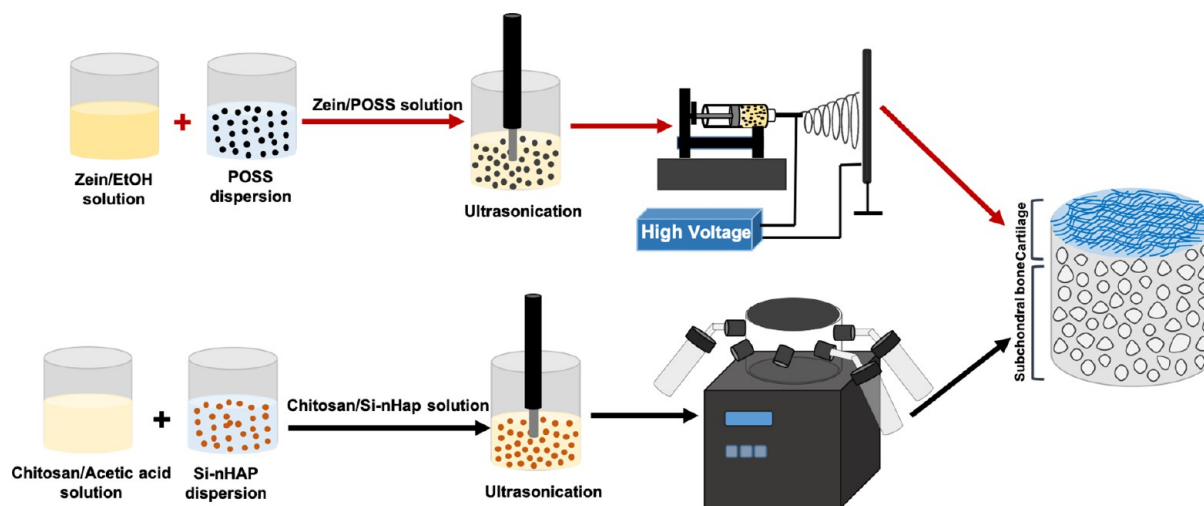
Figure 1. Schematic process of the chitosan/nHap porous layer and zein/POSS fiber layer.

lyophilized for 48 h (−46 °C, 0.01 mbar). Freeze-dried scaffolds were stored in a desiccator after fabrication (Figure 1).

Preparation of the Zein/POSS Fiber Layer. The zein solution and POSS dispersion were prepared separately. The zein (25% w/v) solution was dissolved in 70% (v/v) EtOH, and POSS (20% w/w) nanoparticles were dispersed in 70% (v/v) EtOH. Then, POSS dispersion was added to the zein solution, followed by continuous stirring for 1 h. The zein/POSS solution was electrospun in a 2 kV/cm electric field with a distance of 10 cm at a 5 mL/h feeding rate with a power supply (Gamma High Voltage) and syringe pump (New Era Pump Systems Inc.) (Figure 1).

Preparation of the Chitosan/Si-nHap-Zein/POSS Bilayer Scaffold. Chitosan/Si-nHap porous structures were fixed on the collector of an electrospinning system with double-sided aluminum tape, and the zein/POSS solution was electrospun on the porous layer.

Characterization of Chitosan/Si-nHap-Zein/POSS Bilayer Nanocomposites. *Morphology. Stereomicroscopic Examination.* The morphologies of the porous and fiber layers of a dry scaffold were viewed with a stereomicroscope (Olympus SOIF DA 0737). The stability of the bilayer scaffold was examined in wet conditions. Porous and bilayer scaffolds were incubated in 1× PBS solution, and the integration of the porous and fiber layers was observed under a stereomicroscope.

SEM Analysis. Bilayer nanocomposite scaffolds were analyzed with scanning electron microscopy (FEI Quanta FEG 250) to investigate the effect of nanoparticles on surface morphology and determine the average pore size and fiber diameter. Scaffolds were sputter coated with a thin gold layer (Emitech K550X). ImageJ software was used for average pore size and fiber diameter measurements.

Particle Size Determination with Dynamic Light Scattering (DLS) Analysis. Hydrodynamic sizes of the Si-nHap and POSS nanocage were evaluated with a Malvern Zetasizer (Nano ZS). Nanoparticles (1% w/v) were dispersed in deionized water, and dispersed samples were incubated in an ultrasonic bath for 5 min to prevent agglomerations before analysis.

X-ray Diffraction (XRD) Analysis. XRD analysis was performed to observe the crystal structure of Si-nHap and POSS nanoparticles incorporated in each polymer layer. The intensity was measured between 5 and 60° (2θ) with a scanning rate of 0.02°/sec (Philips X'PertPro).

Fourier Transform Infrared Spectroscopy (FT-IR) Analysis. The chemical structure of each layer and the interaction of a nanoparticle incorporated in the polymer matrix were analyzed using an ATR attachment (PerkinElmer, UATR Two) at a wavelength range from 4000 to 650 to cm^{-1} and 2 cm^{-1} resolution.

Contact Angle Measurement. The static air/water contact angles of fiber and porous layers were measured with an optical tensiometer (Attension Theta Lite). Ultrapure water was used with 5 μL working

volume. Contact angle data of each layer were evaluated as the mean value of five different measurements.

Porosity Determination with the Liquid Displacement Method. The liquid displacement method is used to measure the porosity of the scaffolds. The scaffolds (W) were immersed in a graduated cylinder containing a known volume (V_1) of ethanol. The cylinder is placed in a vacuum to force the ethanol into the pores of the scaffold until no air bubbles emerged from the scaffold. The total volume of the ethanol and scaffold is then recorded as V_2: the volume difference ($V_2 - V_1$) is the volume of the skeleton of the scaffold. Then the scaffold is removed from the ethanol, and the residual ethanol volume is measured as V_3. The total volume of the scaffold, V, is then $V = V_2 - V_3$. The porosity of the open pores in the scaffold, ε, is evaluated as

$$\varepsilon = (V_1 - V_3)/(V_2 - V_3) \tag{1}$$

Compression Test. The mechanical strength of bilayer nanocomposite scaffolds was evaluated with a compression test (ASTM-D 5024-95a) using a texture analyzer (TA XT Plus, Stable Micro Systems). Experiments were carried out with five specimens of each group. Samples were tested with up to 75% of original height with 5 mm/min cross-head speed. Elastic modulus (E) was calculated using stress−strain curves.

Swelling Study. A swelling study was performed to investigate the water uptake capacity of a bilayer nanocomposite. Scaffolds were weighed in dry conditions (W_d) and then incubated in 1× PBS (phosphate buffered saline) solution at 37 °C for 24−48 h. After the incubation periods, wet scaffolds were weighed (W_w). The swelling ratio (SR) was calculated with the following equation:

$$SR = W_w - W_d/W_d \tag{2}$$

Enzymatic Degradation. Enzymatic degradation of bilayer nanocomposite scaffolds was determined by the incubation of samples in enzymatic lysozyme solution at 37 °C; 1.5 μg/mL lysozyme obtained from chicken egg whites was used in order to mimic human serum.[38] Sodium azide (0.01%) was added to the enzymatic solution to inhibit microbial growth. The enzymatic solution was refreshed every 48 h periods to ensure continuous enzyme activity. Scaffold weight loss (%) was evaluated for the seventh and 14th day incubation periods. Biodegradation was determined as weight loss % calculated using eq 3;

$$\text{weight loss \%} = \frac{W_o - W_1}{W_o} \tag{3}$$

In Vitro Studies. Cell Cultivation. MG-63 osteosarcoma and SW-1353 chondrosarcoma cells were inoculated on each layer simultaneously with a double-sided manner. Scaffolds were sterilized at 50 °C with ethylene oxide prior to inoculation. Cell seeding on layers was carried out with 1 × 10^6 cells/μL for each sample (2 mm × 2 mm × 2

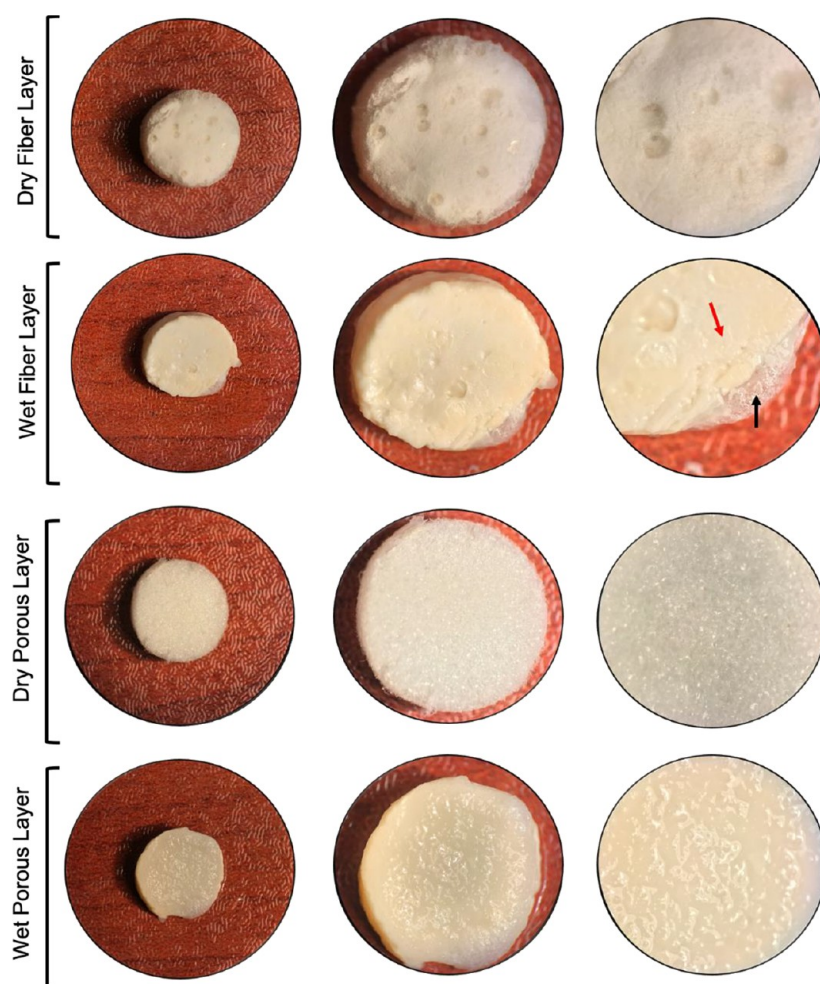**Figure 2.** Stereoimages of fiber and porous layers composed of bilayer scaffolds in dry and wet conditions (1×, 2×, and 4× magnifications, respectively).

mm). First, MG-63 cells were inoculated on the porous chitosan/SinHap composite surface, and their adhesion was provided by means of incubation for 30 min. Then, SW-1353 chondrosarcoma cells were seeded on the zein/POSS fiber surface. Cells were cultured with MEM-Eagle medium consisting of 10% FCS, L-glutamine, and penicillin-streptomycin-amphotericin B. The culture medium was refreshed twice a week. The experiments were repeated three times for each group.

Cell Viability and Proliferation by LDH and Resazurin Assays. A Resazurin cell viability kit was used to measure the metabolic activity of the cells cultivated on bilayer composite scaffolds. Resazurin was used with phenol red-free medium. After 3 h of incubation, the cell viability was measured by a fluorometric measurement technique in 96-well plates (Ex = 530−570 nm, Em = 590−620 nm). In addition, an LDH toxicity test (Thermofisher Scientific) was used to investigate the toxicity during culture.

Alkaline Phosphatase Activity (ALP) Assay. Osteogenic differentiation of MG-63 cells was detected with ALP expression. Extracellular ALP secretion was measured spectrophotometrically (Thermolab Systems, Multiskan Spectrum) using an Enzyline ALP kit (Biomerioux Inc.) for each scaffold. The measurement was performed at 405 nm according to the kit protocol.

Determination of Glycosaminoglycan (GAG) Secretion. In this study, GAG production was used as a chondrogenic differentiation marker. The GAG secretion of SW-1353 cells was measured spectrophotometrically with a proteoglycan detection kit (Amsbio-AMS Biotechnology). GAG extraction was performed with the papain extraction method according to the manufacturer's protocol.

Determination of Cell Attachment with Florescence Microscopy and Scanning Electron Microscopy (SEM). MG-63 and SW1353 cells were inoculated on porous and fiber layers for 7 days. Cell fixation was carried out with paraformaldehyde (3.7% v/v) before staining. After fixation, samples were washed with 1× PBS and permeabilized with Triton X-100 (0.1%) for florescence staining. Progressively, cells fixed on the layers of scaffolds were stained with DAPI and Alexa Fluor 555 and observed with florescence microscopy (Zeiss Observer Z1). Before SEM analysis, fixed scaffolds were incubated in a graded ethanol series (50−100%) to remove aqueous PBS solution and dry samples.

Histologic Staining. Sample fixation was carried out with 10% formalin for 72 h, and the samples were embedded in paraffin after routine light microscopic tissue tracking processes. Scaffold sections with a thickness of 5 μm were retrieved from paraffin blocks (LEICA RM 2255). Scaffold sections were left at 60°C for 30 min for deparaffinization for all staining protocols.

Hematoxylin-Eosin (H&E) Staining. After deparaffinization, sections were exposed to xylol three time at room temperature: the first one for 20 min and the other two for 10 min each. Later, they were passed through 2 different absolute alcohols and alcohol series reducing from 96% to 70% for the rehydration process. After the cross sections were rinsed with distilled water, they were stained with hematoxylin (01562E, Surgipath) for 10 min. The cross sections were washed with running water for 10 min to remove excess hematoxylin and stained with eosin (01602E, Surgipath) for 2 min. After these staining protocols, sections immersed in 70%, 80%, 96%, and two series of 100% ethanol, then they were closed with Entellan (UN 1866, Merck) after being kept in three variances of xylol (20 min for each variance) to make pellucid.

Masson's Trichrome (MT) Staining. Deparaffinized sections were kept in three different xylenes: the first of which for 30 min and the
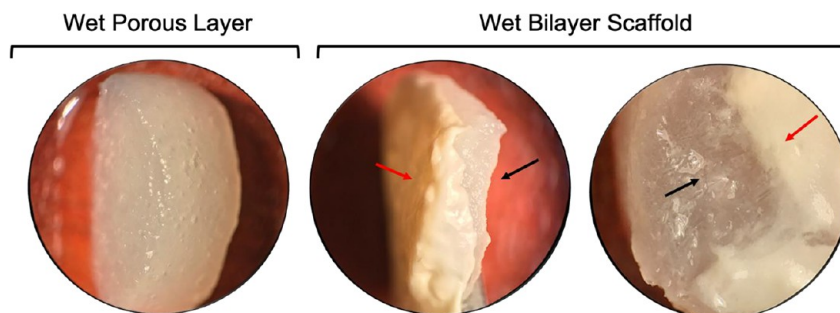
Figure 3. Stereoimages of wet bilayer scaffolds with a cross-sectional view (2× and 4× magnifications).
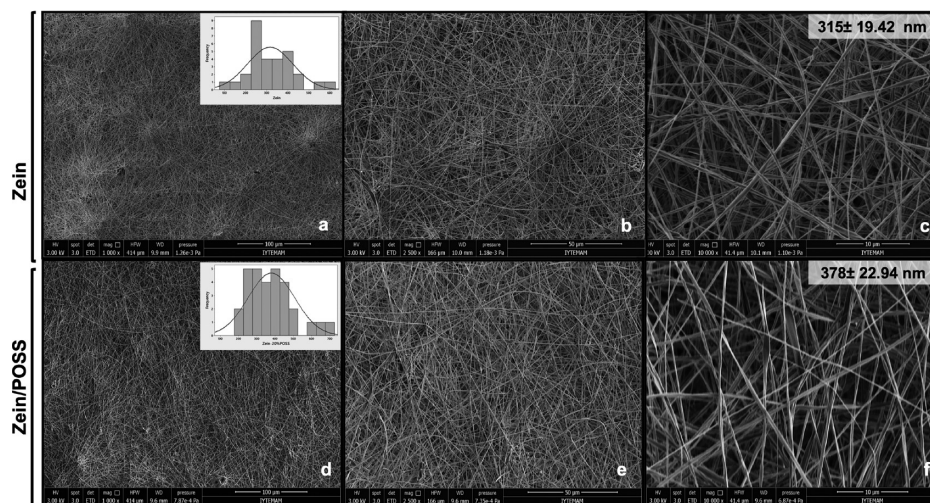

Figure 4. SEM images of fiber layers: zein (a−c) and zein/20% POSS (d−f) with histograms of the fiber diameter distribution and average fiber diameters for each group.
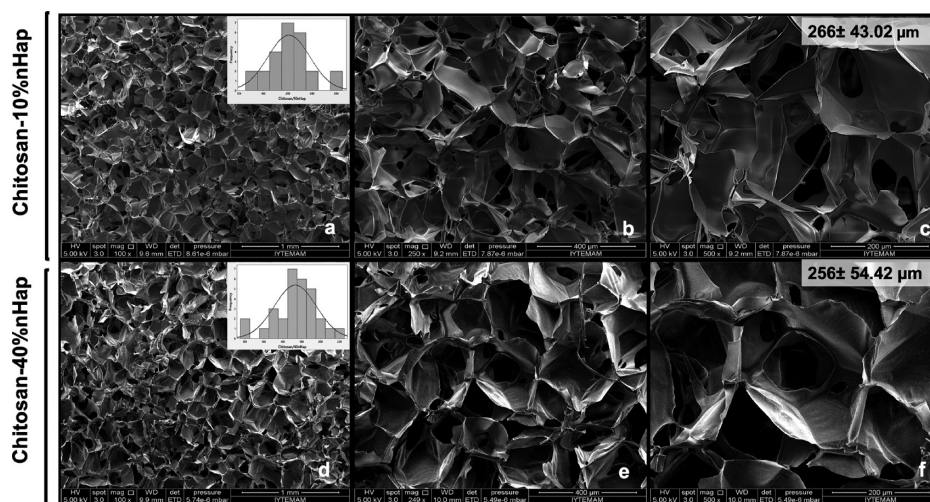

Figure 5. SEM images of porous layers: chitosan/10% nHap (a−c) and chitosan/40% nHap (d−f) with histograms of the pore size distribution and average pore sizes for each group.

other two for 20 min each. Then they were passed through 2 different absolute alcohol and alcohol series reducing from 96% to 70% for the rehydration process. After being kept in distilled water for 5 min, they were stained with a Masson's trichrome staining set (Bio-Optica) with respect to the kit protocol. Scaffold sections were passed through distilled water and the graded ethanol series and incubated in 100% ethanol for 1 min. Finally, sections were closed with Entellan after the process of making pellucid with xylene.

Periodic Acid Schiff (PAS) Staining. After deparaffinization, sections were kept in three different xylenes: the first one was for 30 min in an incubator and the other two were for 20 min. After this step, sections were passed through 2 different absolute ethanol solutions and ethanol series reducing from 96% to 70% for the rehydration process. Then they were immersed in distilled water. Sections were kept in a periodic acid solution for 2 min and washed with distilled water. Then, they were stained with Schiff solution for 15 min. After being washed with running water for 5 min, the nuclei were stained with Mayer hematoxylin

(01562E, Surgipath) for 30 s and were taken into running water. The samples, which were kept in running water for 5 min, were rinsed with absolute ethanol.

Collagen Type 1 and Collagen Type 2 Immuno-Histochemical Staining. Sections, which were deparaffinized for immunohistochemical examination, were brought into distilled water after being rehydrated in a graded ethanol series. Surroundings of scaffold sections were limited with dakopen (Dako, Glostrup, Denmark). Hydrogen peroxide (3%) was applied on the section for 10 min, which was kept waiting in trypsin at 37 °C for 15 min to inhibit the endogenous peroxidase. Collagen type 1 and col type 2 primary antibodies (Sigma-Aldrich) were applied on sections without washing, which were washed with PBS and incubated with blocking solution at room temperature for 30 min. Sections were kept at +4 °C overnight. Then, scaffold sections were incubated with biotinylated secondary antibody and subsequently with the avidin−biotin complex (streptavidin) for 30 min each. Diaminobenzidine (DAB) was used for visibility of the reaction. Background staining was carried out with Mayer's hematoxylin (01562E, Surgipath). Samples were closed with Entellan (UN 1866, Merck, after the process of dehydration and pellucid formation.

Statistical Analysis. All experiments were carried out in triplicate, and data were given as means ± standard deviation (SD). Statistical analyses were carried out with Graphpad Prism 7 software. One-way and two-way analysis of variance (ANOVA) tests were used to assess the significant differences between experimental groups with a $p < 0.05$ significance level.

RESULTS AND DISCUSSION

Morphology and Porosity Determination. Structural integrity and stability of bilayer scaffolds were investigated with stereomicroscopy. Images indicated that the fiber layer is physically integrated in the porous sublayer in both dry and wet conditions (Figure 2). Cross-sectional images of bilayer scaffolds also demonstrated that the zein-based fiber layer and chitosan-based porous layers showed a good compatibility (Figure 3). The structure and morphology of bilayer scaffolds were examined by SEM, and images were analyzed by the ImageJ program to determine the average pore size of the sublayer and the fiber diameter of the upper layer. In addition, the nanofiber structure of the zein/POSS upper layer and the microporous structure of the chitosan/Si-nHap sublayer were observed with SEM analysis (Figures 4 and 5). The average pore size and fiber diameter of layers with different Si-nHap and POSS (%) contents were depicted in Table 1. The minimum pore size

Table 1. Porosity % of the Chitosan/Si-nHap Sublayer

porous layer	porosity (%)
chitosan	84 ± 2.7
chitosan/10% Si-nHap	86 ± 0.8
chitosan/40% Si-nHap	85 ± 1.1

required for a scaffold is regarded as approximately 100 μm to provide the appropriate microenvironment and nutrient transport. Besides, the average pore size range must be between 200 and 350 μm for optimum bone tissue growth.[39] Si-nHap particle dispersion in a chitosan matrix was depicted in Figure 6. SEM images of the porous layer demonstrated that increasing the Si-nHap concentration altered the surface and, however, did not affect the pore size (252−266 μm), which was found appropriate for bone cell proliferation, tissue ingrowth, nutrient delivery, and bone tissue vascularization.[40,41]

The porosity of the chitosan/Si-nHap sublayer was evaluated with the liquid displacement method. Results indicated that highly porous structures (85%) were fabricated with a lyophilization technique (Table 1) and found appropriate for

the trabecular bone, which has an interconnected porous structure with a porosity range between 50 and 90%.[42] Si-nHap incorporation did not alter the pore structure and total porosity of chitosan scaffolds. SEM images with the backscatter mode also showed that Si-nHap particles were homogeneously distributed on the pore wall surface (Figure 6). Besides, increasing Si-nHap content from 10% to 40% did not affect the distribution negatively due to the ultrasonic homogenization used for homogeneous distribution of Si-nHap particles in a chitosan matrix.

A homogenous nanofiber matrix was obtained from electrospinning zein/POSS nanocomposites. POSS nanocages did not alter the zein fiber morphology. This can be attributed to the homogeneous distribution of POSS nanocages in the zein matrix, and 20% POSS nanocage incorporation to the zein matrix increased the diameter of nanofibers from 315 to 378 nm. The bilayer structure composed of chitosan/Si-nHap and zein/POSS layers obtained with a thickness of 38.5 ± 6.5 μm is depicted in Figure 7. SEM images showed that the zein/POSS nanofiber layer was successfully electrospun on a microporous chitosan/Si-nHap layer, coating the surface of pores. The bilayer structure was successfully fabricated to mimic the bone−cartilage interface by combining the porous and fibrous morphology.

Average hydrodynamic size distributions of POSS and Si-nHap particles were measured with DLS analysis. The results indicated that dispersed Si-nHap particles found with an average hydrodynamic size of 168 nm. POSS nanocages generally tend to agglomerate due to the strong interaction between their reactive R groups. Thus, 30% of POSS nanoparticles were observed nonaggregated with an average diameter of 1 nm, which is also in agreement with literature data.[47] However, high percentage POSS nanoparticles were mostly found as aggregated forms (>65%). In addition to these big aggregations, a dispersed POSS solution comprised of small aggregations (5%) with an average size of 10.42 nm shares a similar result with that found in the literature.[48]

Chemical Characterization. XRD patterns of fiber and porous layers showed the characteristic peaks of both the polymer matrix and bioactive agents in composite structures (Figures 8 and 9). The XRD pattern of Si-nHap was depicted in Figure 8a with reference to the reflections of apatite. Chitosan showed characteristic diffraction peaks at 10° and 20°. Characteristic diffraction peaks of both chitosan and Si-nHap were observed in the chitosan/si-nHap composite structure. Characteristic peaks of the POSS nanocage are known as 6.65°, 10.79°, and 18.76° due to its crystalline structure (Figure 9a) as indicated in the literature.[43,44] The zein matrix showed two broad characteristic peaks at 9° and 20° (Figure 9b).

FT-IR analyses of each layer were performed to investigate the interaction of Si-nHap and POSS nanoparticles with polymer matrices (Figures 10 and 11). FT-IR spectra of Si-nHap particles showed characteristic bands of hydroxyapatite with regard to the $(PO_4)^{3-}$ group at 990 (v1), 1030 (v3), and 1100 cm^{-1} (v3). In addition, $(CO_3)^{2-}$ bands were observed at 1450−1500 cm^{-1} as A-carbonation in the hydroxyl site. Si-doped hydroxyapatite showed a small peak for hydroxyl stretching bands at 3600 cm^{-1}.[45−48] Characteristic peaks of chitosan were observed as N−H bending at 1580 cm^{-1} and NH_2 peaks at 1580−1640 cm^{-1}. Stretching vibrations of OH groups were observed at 3547−2850 cm^{-1}. C−O stretching bands were observed at 1030 cm^{-1}.[49] FT-IR spectra of the chitosan/Si-nHap composite showed that characteristic peaks of Hap were obtained in the
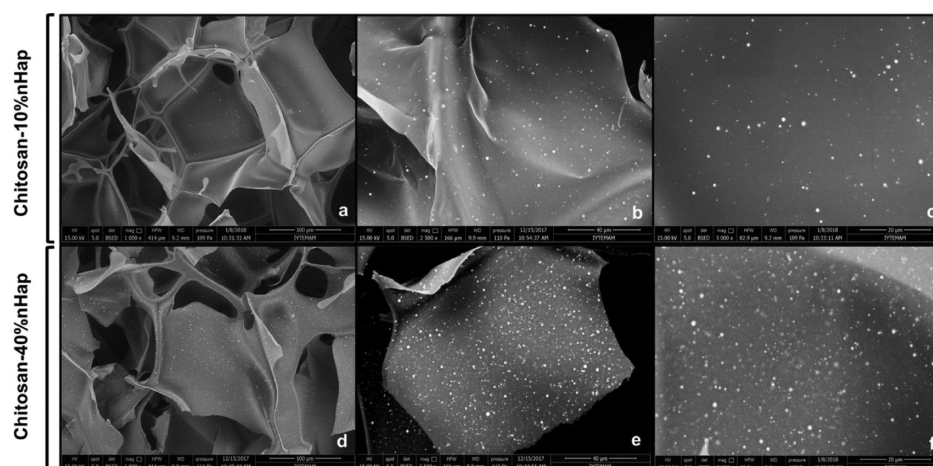
Figure 6. SEM images of the surface morphology of chitosan/10% nHap (a–c) and chitosan/40% nHap (d–f) composite scaffold.
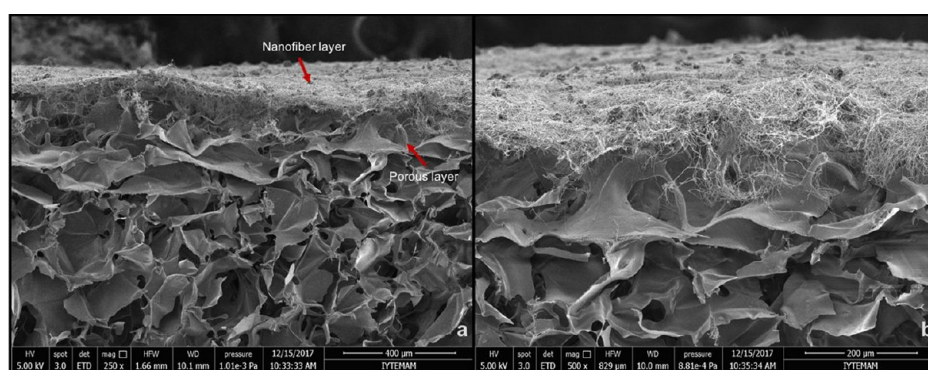

Figure 7. SEM images of bilayer scaffolds: top view and cross section with different magnifications (a, b). The nanofiber layer was electrospun on a microporous sublayer.

composite structure with a lower intensity at 1050 cm^{-1}, overlapping with the C−O stretching bands of chitosan.

FT-IR spectra of the zein matrix and POSS nanoparticles were demonstrated in Figure 11. Octa-TMA POSS is composed of a rigid Si−O cage with eight $ON(CH_3)_4$ groups in each corner of the cage structure. FT-IR peaks of Octa-TMA POSS indicate that the silsesquioxane inorganic cage structure has a strong, symmetric Si−O−Si stretching band at 990−1100 cm^{-1}. The absorbing peaks of the reactive R group (tetramethylammonium) were observed at 1680 and 1480−1490 cm^{-1} as stretching vibrations. Characteristic peaks of zein were observed at 1656 cm^{-1} as the amide I vibration mode, which indicated the α-helix structure of zein and at 1540 cm^{-1} as amide II vibration modes. In addition, peaks observed at 2960 and 2928 cm^{-1} were attributed to C−H stretching with regard to the CH and CH_2 functional groups of zein. The hydroxyl stretching vibration in zein was observed at 3290 cm^{-1} as a broad band.[50,51]

Surface Wettability. Surface hydrophilicity has been considered as a significant factor for cell−biomaterial interaction. Thus, the wettability of each layer composing the scaffold was analyzed, and the contact angle data were depicted in Table 2. Zein contains an almost equal amount of hydrophilic and hydrophobic amino acids with its amphiphilic character.[52] During the electrospinning process, hydrophobic amino acids of zein are located on the outer side and interact with the solution droplet due to the rapid solvent evaporation.[53,54] Therefore, the zein fiber layer possessed a moderately hydrophilic characteristic with 76°. POSS incorporation did not significantly alter the

surface characteristics of zein fibers. The chitosan porous layer was pressed as thin sheets to perform contact angle measurements. The chitosan matrix and chitosan/Si-nHap composite also showed a moderately hydrophilic surface characteristic with 83° and 85°, respectively. Generally, highly hydrophilic and hydrophobic surfaces affect the cell−material interaction negatively. In literature, materials showing a moderately hydrophilic characteristic were found to be appropriate for protein adsorption and subsequently cell adhesion.[55,56] Therefore, the contact angle results of porous and fiber layers were found to be favorable for protein adsorption and cell interaction. Surface topography is very important for contact angle measurements, since the static contact angle of a material surface is significantly affected by surface alterations at a microscale, which create a barrier on the material surface.[57] Thus, the positive effect of hydrophilic octa-TMA POSS and Si-nHap on surface wettability could not be observed properly.

Swelling Properties. The swelling ratio of monolayer and bilayer scaffolds was examined for 24 and 48 h of incubation (Table 3). The results showed that increasing the Si-nHap particles did not significantly affect the water absorption capacity of porous chitosan scaffolds. In addition, zein nanofiber layers electrospun on porous chitosan/Si-nHap composites did not alter the swelling ratio of scaffolds. However, POSS incorporation to the nanofiber layer increased the water absorption capacity of chitosan/10% nHap scaffolds due to the hydrophilic structure of POSS nanocages. The similar enhancing effect was not observed on chitosan/40% Si-nHap composites. Studies
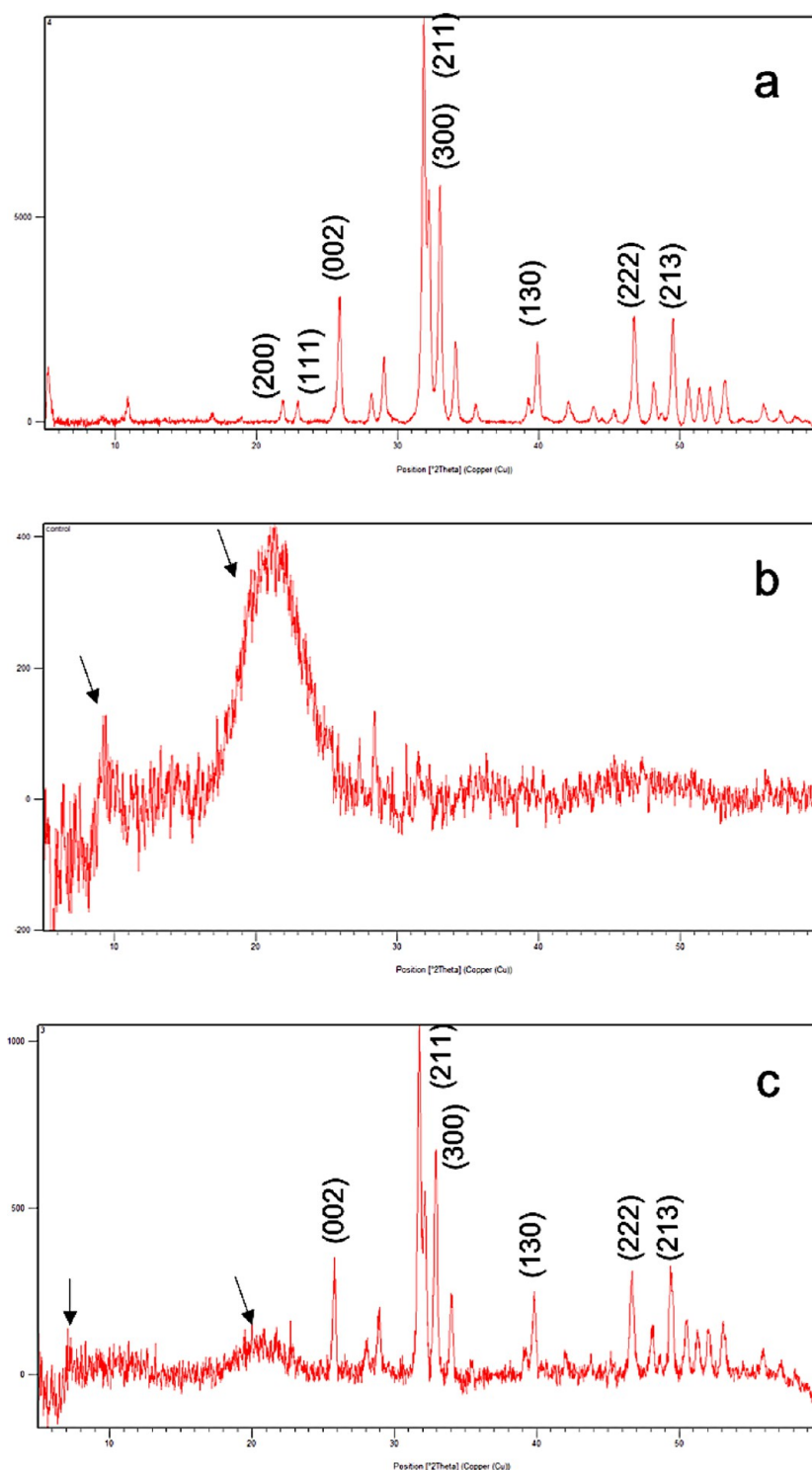
Figure 8. XRD spectra of Si-nHap (a), chitosan (b), and chitosan/Si-nHap (c).

indicated a similar decreasing effect of water absorption capacity with the addition of Hap on chitosan scaffolds.[58−60]

Mechanical Properties. Generally, Si-nHap incorporation improves the mechanical properties of bone grafting materials.[61] The mechanical response of chitosan/Hap composites can alter with the effect of particle size and particle size distribution of hydroxyapatite particles concerning the interfacial interactions between the chitosan matrix and hydroxyapatite particles. The compression test results showed that Si-nHap particles showed a good distribution in the structure (Figure 12a). Therefore,

increasing the Hap content enhanced the moduli of scaffolds. Besides, nanoparticles form a tighter interface when incorporated in a polymer matrix due to having a large surface area,[62] Compression test results indicated that increasing Si-nHap % content in the chitosan matrix increased the compression moduli of scaffolds from 79 to 128 kPa (62%). In a study, Hap particles were incorporated to chitosan/collagen/hyaluronic acid blends, and the effect of Hap particles on mechanical properties was observed. Similarly, they found that the addition
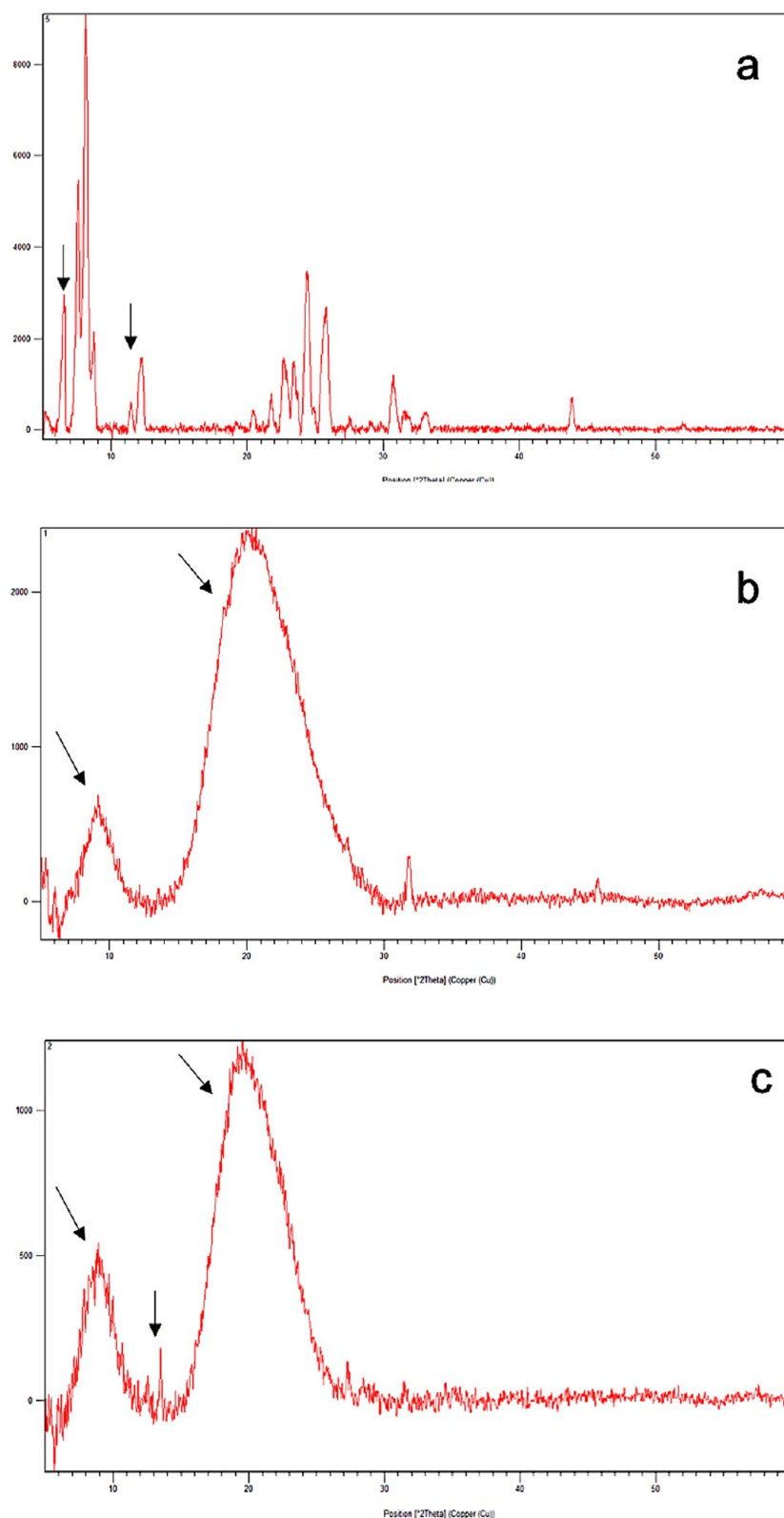
Figure 9. XRD spectra of POSS (a), zein (b), and zein/POSS (c).

of hydroxyapatite up to 80% enhanced the mechanical strength of scaffolds.[63]

Enzymatic Degradation. An enzymatic degradation study was carried out to determine the degradation behavior of bilayer scaffolds for the 14th day of incubation in a simulated body fluid containing lysozyme. The increase in Si-nHap content

decreased the weight loss % of scaffolds composed of the porous chitosan/Si-nHap and zein/POSS nanofiber layer for the seventh day of incubation. This may result from the homogeneous particle distribution and reinforcing effect of Si-nHap in the polymer structure (Figure 12b). However, POSS incorporation to the nanofiber layer increased the weight loss %
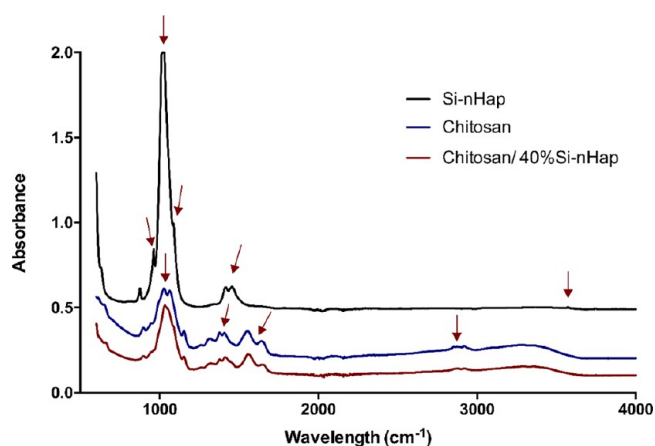
Figure 10. FT-IR spectra of Si-nHap particles, porous chitosan, and chitosan/Si-nHap composite layer.
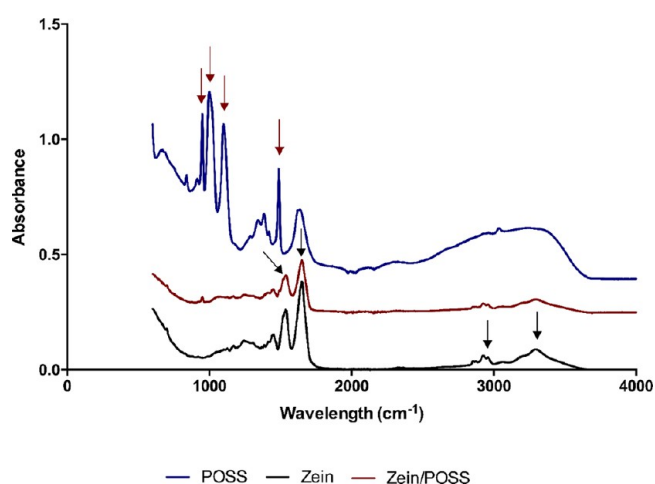

Figure 11. FT-IR spectra of zein, zein/POSS fiber layer, and POSS nanoparticles.

Table 2. Static Air/Water Contact Angle of Porous and Fiber Layers

groups	contact angle (deg)
chitosan	83 ± 0.8
chitosan/40% Si-nHap	85 ± 0.9
zein	76 ± 5.1
zein/POSS	79 ± 2.2

Table 3. Swelling Ratio of Bilayer Scaffold Groups for 24−48 h Incubation Time

monolayer scaffolds	swelling ratio (24 h)	swelling ratio (48 h)
chitosan	21.3 ± 1.5	20.8 ± 0.1
chitosan/10% Si-nHap	18.5 ± 0.9	17.7 ± 0.6
chitosan/40% Si-nHap	20 ± 1.2	16 ± 0.5
bilayer scaffolds	swelling ratio (24 h)	swelling ratio (48 h)
chitosan/10% Si-nHap-zein	23 ± 2	23.2 ± 2.1
chitosan/40% Si-nHap-zein	19.4 ± 0.4	19 ± 0.3
chitosan/10% Si-nHap-zein/POSS	34.6 ± 4.6	35.5 ± 5.8
chitosan/40% Si-nHap-zein/POSS	21.7 ± 0.6	22 ± 1.3

of bilayer scaffolds on the seventh day due to the degradation of organic R groups in POSS nanocages and dissolution of POSS silica nanocages from the nanofiber surface. Besides, incorporation of silicate-based nanoparticles shows an inducing effect on the water uptake capacity of a polymer matrix. This leads to alterations on the surface and bulk properties of the polymer and changes the degradation behavior by accelerating the weight loss of the composite.[64] Thus, composite scaffolds possess a higher water absorption capacity, causing the hydrolytic attack in the structure.

***In Vitro* Studies.** *In vitro* cell culture studies were performed on bilayer scaffolds composed of chitosan/40% Si-nHap/zein as a control and chitosan/40% Si-nHap/zein-POSS. MG-63 and SW-1353 cells were cultured on bilayer scaffolds. LDH assessment showed the concentration of the damaged cells in the plasma membrane, and it was used to measure the initial effect of the scaffolds on the viability of seeded SW 1353 and MG-63 cell lines. Results indicated that there was not a decrease in the mitochondrial activity, and the scaffolds did not display a toxicity during the culture period (Figure 13a). There was no significant difference in the levels of LDH during the culture period. Levels of initial cell death were similar on all scaffolds, and the POSS incorporation did not significantly increase cell death. This correlated with the cell proliferation results. MG-63 osteosarcoma and SW-1353 chondrosarcoma cell proliferations were evaluated with a resazurin assay. Cell viability % increased on the third, seventh, and 14th days. However, statistically no significant difference was observed between both groups (Figure 13b). ALP, as a cell surface glycoprotein, is one of the important markers for osteoblastic differentiation, acting in biomineralization.[65,66] The differentiation behavior of MG-63 cells, as expressed by the ALP activity after 7 days of culture on the scaffolds, followed a similar trend to that of the proliferation behavior. These ALP expression levels, alongside the proliferation behaviors, provide a good illustration of the improved osteogenic potential of a porous chitosan matrix due to the Si-doped nHap incorporation. Bilayer scaffolds exhibited increasing ALP activity levels, leading to significant early osteogenic differentiation on the 14th day of incubation (Figure 13c). Similarly, SiO_2 particle incorporation in chitosan/gelatin scaffolds showed an inducing effect on ALP activity at an early period of incubation and caused faster differentiation of osteoblast-like cells on scaffolds.[67]

Collagen and GAG are the major ECM components for cartilage tissue, and these proteins are secreted during chondrogenesis. Thus, they were used as a measure of chondrocyte function.[36] The data showed that SW1353 cells grown on zein/POSS nanocomposites produced a high amount of GAG in their surrounding ECM when compared to the zein fiber layer. The GAG secretion differences were found to be statistically significant for both the 21st day and 28th day of incubation (Figure 13d). A maximum GAG secretion was observed at day 21 of incubation. Gomez-Sanchez et al. investigated the effect of PEG−POSS incorporation to the PLLLA matrix for chondrogenic differentiation and indicated that GAG secretion slightly increased on PLLA fibers containing PEG−POSS compared to control group.[68] *In vitro* results indicated that Si incorporation provided an enhancing effect for both osteogenic and chondrogenic differentiation of MG-63 and SW1353 cells. Similarly, Bunpetch and co-workers investigated the effect of silicate-based scaffolds for dual regeneration of bone and cartilage tissue at osteochondral defects. *In vitro* results indicated that Si incorporation promoted osteogenic differ-
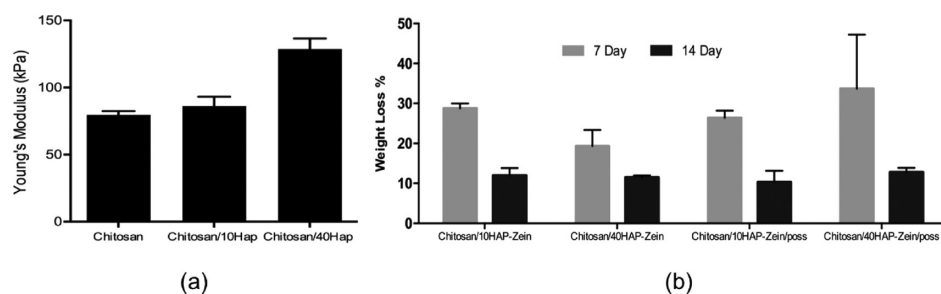
Figure 12. Compression modulus (a) and weight loss % of bilayer scaffolds on the 7th and 14th day (b).
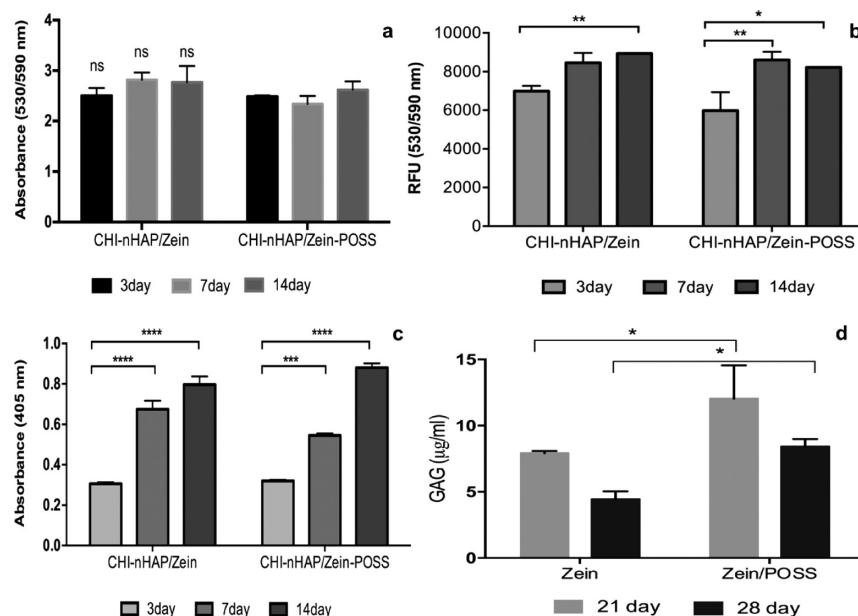

Figure 13. *In vitro* study results of MG-63 osteosarcoma and SW1353 chondrosarcoma cells seeded on bilayer scaffolds. Cytotoxicity with the LDH assay (a). Proliferation with the rezasurin assay (b). ALP activity (c). GaG content (d).
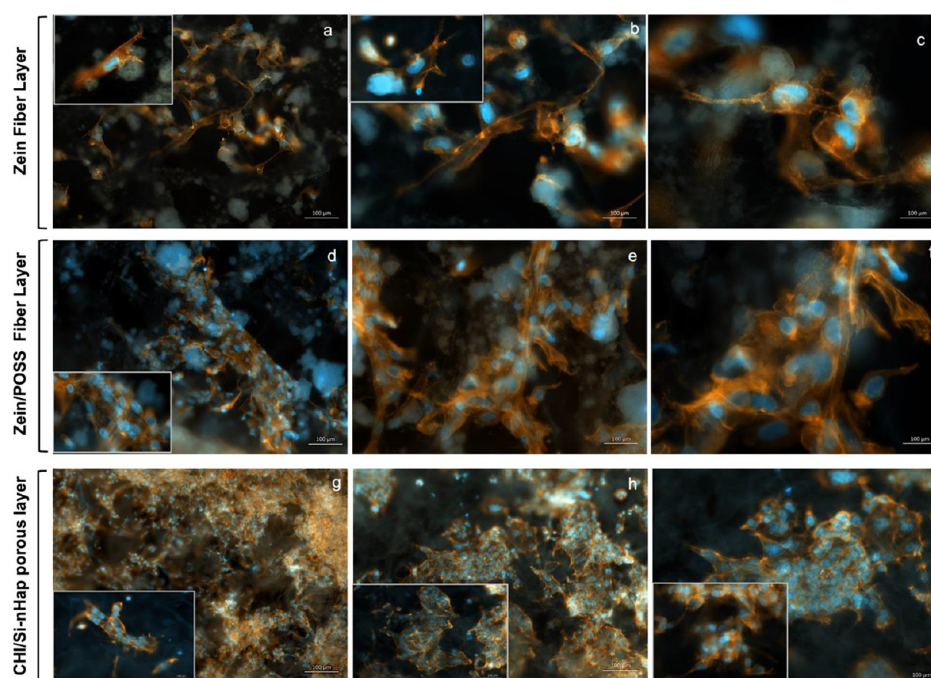

Figure 14. Florescence images of MG-63 cells and SW1353 cells on the 7th day on nanofiber and microporous layers, respectively. Cell attachment for the control group on the 7th day (a−c). Cell attachment for the POSS-incorporated group (d−f) on the 7th day, (g−i) for CHI/Si-nHap.
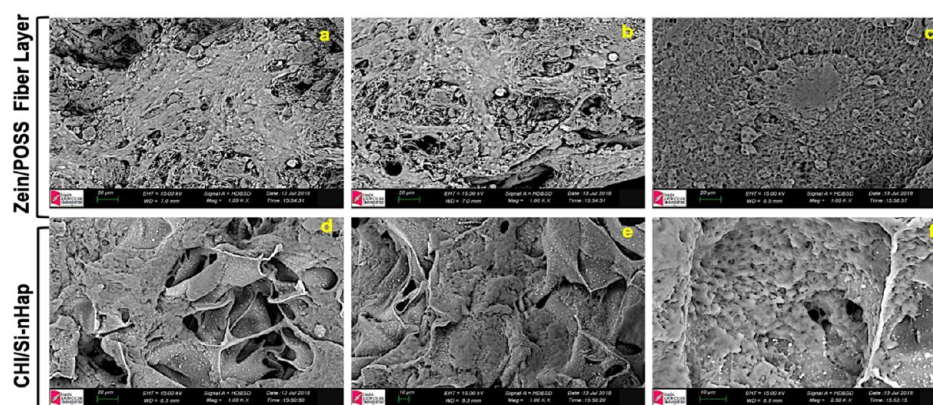
Figure 15. SEM images of SW-1353 and MG-63 cells on the POSS-incorporated zein layer (a−c) and chitosan/40% Si-nHap scaffold (d−f).
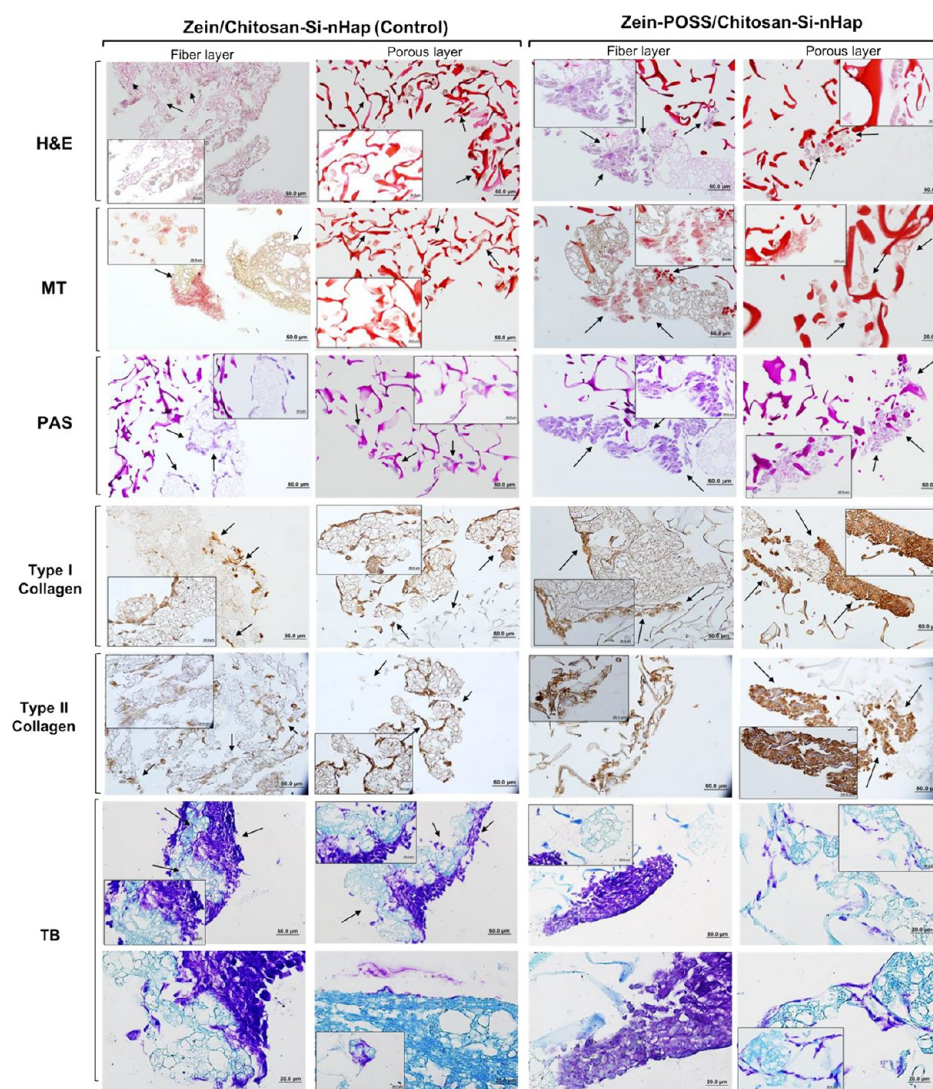

Figure 16. Hematoxylin-eosin (H&E), Masson's trichrome (MT), periodic acid Schiff (PAS), toludine blue (TB), and collagen type 1 and collagen type 2 immuno-histochemical staining images of bilayer scaffolds on the 7th day. Control: chitosan/Si-nHap/zein. Bilayer nanocomposite scaffolds: chitosan/Si-nHap/zein-POSS.

entiation of BMSCs and maintained the chondrocyte phenotype.[24]

Our results provide evidence of an increase in cell proliferation in both scaffold types. The MG-63 and SW1353 cell−material interaction on each layer of scaffolds was observed

with florescence microscopy (Figure 14). The nuclei and cytoskeleton of cells were stained with DAPI and Alexa Fluor 555, respectively. Florescence images showed favorable cell attachment and proliferation on each layer. The zein nanofiber layer provided a suitable microenvironment for SW-1353 cells
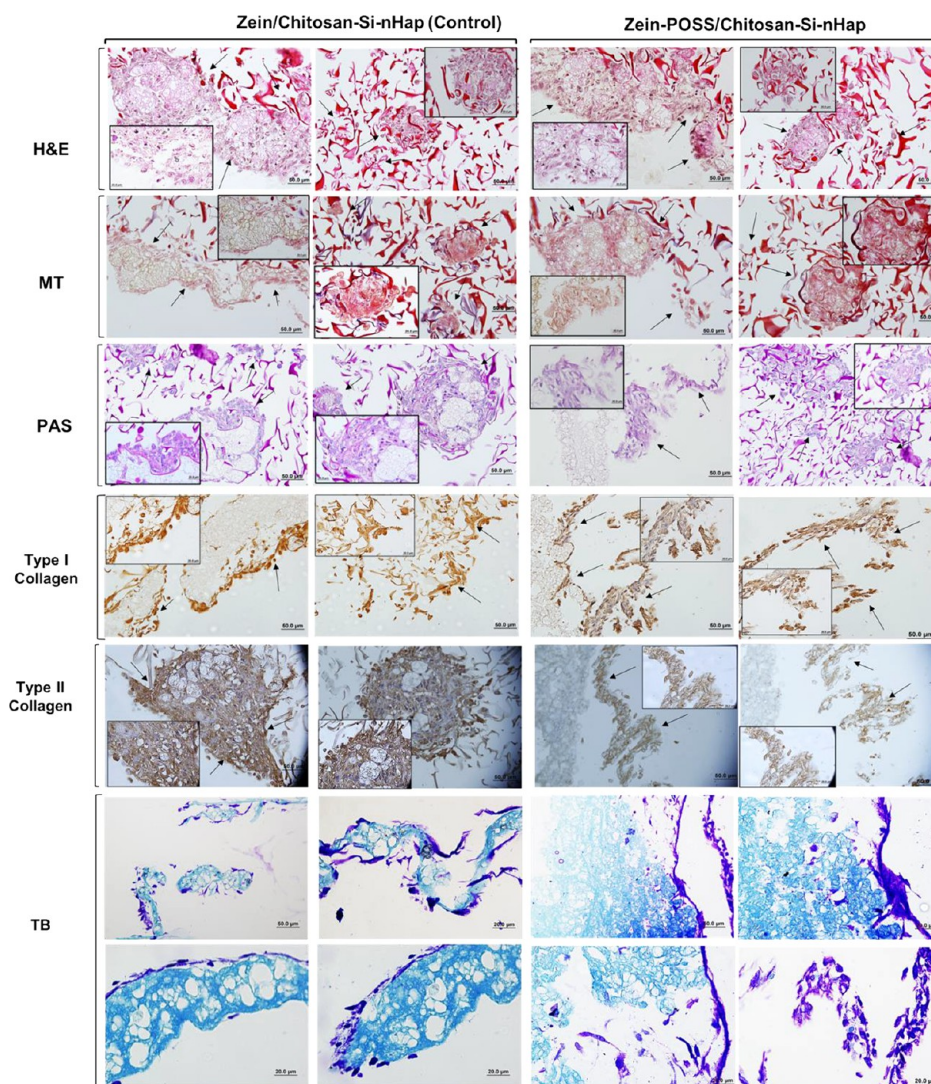
Figure 17. Hematoxylin-eosin (H&E), Masson's trichrome (MT), periodic acid Schiff (PAS), toluidine blue (TB), and collagen type 1 and collagen type 2 immuno-histochemical staining images of bilayer scaffolds on the 14th day. Control: chitosan/Si-nHap/zein. Bilayer nanocomposite scaffolds: chitosan/Si-nHap/zein-POSS.

(Figure 14a−c). However, chondrocyte-like cell proliferation significantly increased on the POSS-incorporated zein nanofiber layer on the seventh day (Figure 14d−f). Similarly, Guasti and co-workers investigated the effect of POSS−PCU scaffolds on human adipose tissue-derived stem cells (hADSCs) for chondrogenic differentiation and observed progressive cellularization of the scaffold.[69] DAPI-Alexa Fluor images demonstrated SW-1353 attachment and spreading on the zein nanofiber layer, whereas POSS incorporation enhanced cell attachment and spreading by altering the surface topography and hydrophilicity with its silica cage structure. Osteoblast-like cells (MG-63) also successfully attached on pore walls of the chitosan/Si-nHap porous sublayer, spread, and proliferated by forming clusters (Figure 14g−i). In addition, cell attachment and spreading were observed via SEM analysis (Figure 15). SEM images showed that SW-1353 and MG-63 cells highly proliferated on the POSS-incorporated zein layer and Si-nHap-incorporated chitosan layer, respectively.

Histological Staining. Histological images indicated that MG-63 and SW 1353 cells proliferated on chitosan/Si-nHAp porous and zein/POSS layers. The sections belonging to both the seventh and 14th day of the control and POSS-incorporated

bilayer scaffold groups were assessed histochemically and immunohistochemically. The sections were stained with hematoxylin and eosin (H&E) for the cell morphology with an extracellular matrix formation, Masson's trichrome (MT) for collagen content of the connective tissue matrix, and periodic acid Schiff (PAS) and toluidine blue (TB), which are mainly used to highlight the structures with a high percentage of carbohydrate content such as glycogen, glycoproteins, and proteoglycans typically. Proteoglycans are generally formed by glycosaminoglycans (GAGs), which are attached to the core proteins and found in all extracellular matrixes of connective tissue. H&E, MT, and PAS staining on the seventh day revealed that cell proliferation and matrix formation started to be seen on both fiber and porous layers of scaffolds (Figure 16). Cell clusters were observed on the fiber and porous layers of the control group. A higher cell proliferation and matrix formation were seen on POSS-incorporated zein fibers compared to control group. Images showed that cells started to infiltrate pore structures and that the cells are located in the pores of bilayer scaffolds. MT staining showed that POSS incorporation increased the collagen content on the zein fiber layer compared to the control group. Besides, PAS staining confirmed well-

formed chondrocytes and indicated that higher glycoprotein and proteoglycan contents were observed on POSS-incorporated fiber layers. Immuno-histochemical staining revealed that both collagen type I and type II formation was observed on fiber and porous layers. POSS incorporation enhanced type I and type collagen II expression on the interphase of the porous fiber layer. Type II collagen staining specified that chondrocytes were detected on the fiber layer and porous fiber layer interface.

H&E staining revealed that MG-63 cells migrated through the inner parts of the scaffold and proliferated as clusters on the 14th day. The nteraction of cell clusters with a porous layer could be seen clearly. In addition, POSS nanoparticles increased the cell proliferation on a fiber layer compared to the control group (Figure 17). Chondrocyte and osteoblast cells were aggregated and surrounded by cartilaginous ECM. Histological data showed that both fiber and porous layers mimic the cartilage and bone sections, exhibiting a homogeneous cell distribution and matrix formation. MT staining showed that collagen formation was observed on a porous layer. Bilayer scaffolds were stained red with MT staining due to the presence of chitosan in the structure. Chondrocyte cells on the fiber layers were stained pink. The chondrocyte lineage was seen on the control fiber layer, whereas the chondrocyte population increased on the zein/POSS fiber layer. A major characteristic of cartilage is a high amount of GAG secretion and deposition (15−25%) by mature chondrocytes in the extracellular matrix.[70] In the current study, PAS and TB were used to detect mucopolysaccharides and specifically GAG units, respectively. It is clearly seen that core proteins of proteoglycans determined the localization of GAGs, and proteoglycan formation was clearly seen in POSS-reinforced zein nanofibers after 14 days. Cell migration and proliferation were detected between porous fiber layers. Finally, the distribution and organization of proteoglycans indicated the calcification of the cartilage matrix. Sections from the control and POSS-incorporated bilayer scaffolds were also immune-labeled for type I and type II collagen (Figure 17). In type I and type II collagen immunohistochemical staining, both scaffolds exhibited immunopositivity on scaffolds on the seventh and 14th day. Significantly more cells were attached on the fiber and porous layers of scaffolds on the 14th day compared to the seventh day (Figure 17). Type I collagen formation of osteoblasts seemed to increase especially in porous layers on the 14th day. Type II collagen expression of chondrocytes was detected on the fiber layer and porous fiber layer interface. Our results suggest that chondrocytes may functionalize type II collagen formation as a scaffold substitute by continuously delivering type II collagen and GAGs for osteochondral defects. Therefore, on the basis of the data shown in the immunohistochemical results, we presume that the successful regeneration of the osteochondral defect may arise from the matrix-like effect of collagen and GAGs produced on the bilayer scaffolds proposed in this study.

CONCLUSIONS

The obtained results show that novel bilayer scaffolds mimic the osteochondral tissue and the enhancement effect of POSS nanocage incorporation to bioactivity of chitosan/Si-nHap-zein/POSS bilayer scaffolds for bone and cartilage regeneration. We have shown that the POSS-incorporated bilayer scaffolds were appropriate for MG-63 and SW 1353 cell adhesion, growth, and proliferation and can be applied effectively in the bone–cartilage tissue systems. It was demonstrated that the composition and mechanical properties of the environment affect the migration of the cells. Metabolic activity and fluorescence microscopy images of cells cultured on chitosan/Si-nHap and zein/POSS porous nanofiber layers evidence the improvement of MG-63 and SW 1353 activity due to the silica content of bioactive agents incorporated in the layers of scaffold. In future studies, these scaffold systems, either alone or in combination with other materials, may serve as a platform to investigate the individual components needed to further optimize function for osteochondral defects.

■ AUTHOR INFORMATION

Corresponding Author
*E-mail: fundatihminlioglu@iyte.edu.tr.

ORCID ⊕
Sedef Tamburaci: 0000-0003-3234-226X
Ozcan Ustun: 0000-0002-8240-1515
Hasan Havitcioglu: 0000-0001-8169-3539
Funda Tihminlioglu: 0000-0002-3715-8253

Notes
The authors declare no competing financial interest.

■ REFERENCES

(1) Romeyn, R. L.; Jennings, J.; George Davies, A. J. Surgical Treatment and Rehabilitation of Combined Complex Ligament Injuries. *North Am. J. Sport. Phys. Ther.* **2008**, *3* (4), 212−225.

(2) Cross, L. M.; Thakur, A.; Jalili, N. A.; Detamore, M.; Gaharwar, A. K. Nanoengineered Biomaterials for Repair and Regeneration of Orthopedic Tissue Interfaces. *Acta Biomater.* **2016**, *42*, 2−17.

(3) Cengiz, I. F.; Oliveira, J. M.; Reis, R. L. Tissue Engineering and Regenerative Medicine Strategies for the Treatment of Osteochondral Lesions. In *3D Multiscale Physiological Human*; Springer London: London, 2014; pp 25−47.

(4) Canadas, F.; Marques, A. P.; Reis, R. L.; Oliveira, J. M. *Regenerative Strategies for the Treatment of Knee Joint Disabilities* **2017**, *21*, 213−233.

(5) Lam, J.; Lu, S.; Meretoja, V. V.; Tabata, Y.; Mikos, A. G.; Kasper, F. K. Generation of Osteochondral Tissue Constructs with Chondrogenically and Osteogenically Predifferentiated Mesenchymal Stem Cells Encapsulated in Bilayered Hydrogels. *Acta Biomater.* **2014**, *10* (3), 1112−1123.

(6) Vinatier, C.; Guicheux, J. ScienceDirect Cartilage Tissue Engineering : From Biomaterials and Stem Cells to Osteoarthritis Treatments. *Ann. Phys. Rehabil. Med.* **2016**, *59* (3), 139−144.

(7) Kim, K.; Lam, J.; Lu, S.; Spicer, P. P.; Lueckgen, A.; Tabata, Y.; Wong, M. E.; Jansen, J. A.; Mikos, A. G.; Kasper, F. K. Osteochondral Tissue Regeneration Using a Bilayered Composite Hydrogel with Modulating Dual Growth Factor Release Kinetics in a Rabbit Model. *J. Controlled Release* **2013**, *168* (2), 166−178.

(8) Lu, S.; Lam, J.; Trachtenberg, J. E.; Lee, E. J.; Seyednejad, H.; van den Beucken, J. J. J. P.; Tabata, Y.; Wong, M. E.; Jansen, J. A.; Mikos, A. G.; et al. Dual Growth Factor Delivery from Bilayered, Biodegradable Hydrogel Composites for Spatially-Guided Osteochondral Tissue Repair. *Biomaterials* **2014**, *35* (31), 8829−8839.

(9) Dong, J.; Sun, Q.; Wang, J. Y. Basic Study of Corn Protein, Zein, as a Biomaterial in Tissue Engineering, Surface Morphology and Biocompatibility. *Biomaterials* **2004**, *25* (19), 4691−4697.

(10) Shukla, R.; Cheryan, M. Zein: The Industrial Protein from Corn. *Ind. Crops Prod.* **2001**, *13* (3), 171−192.

(11) Wang, H. J.; Lin, Z. X.; Liu, X. M.; Sheng, S. Y.; Wang, J. Y. Heparin-Loaded Zein Microsphere Film and Hemocompatibility. *J. Controlled Release* **2005**, *105* (1−2), 120−131.

(12) Gong, S.; Wang, H.; Sun, Q.; Xue, S. T.; Wang, J. Y. Mechanical Properties and in Vitro Biocompatibility of Porous Zein Scaffolds. *Biomaterials* **2006**, *27* (20), 3793−3799.

(13) Jiang, Q.; Reddy, N.; Yang, Y. Cytocompatible Cross-Linking of Electrospun Zein Fibers for the Development of Water-Stable Tissue Engineering Scaffolds. *Acta Biomater.* **2010**, *6* (10), 4042−4051.

(14) Park, J. H.; Park, S. M.; Kim, Y. H.; Oh, W.; Lee, G. W.; Karim, M. R.; Park, J. H.; Yeum, J. H. Effect of Montmorillonite on Wettability and Microstructure Properties of Zein/Montmorillonite Nanocomposite Nanofiber Mats. *J. Compos. Mater.* **2013**, *47* (2), 251−257.

(15) Paliwal, R.; Palakurthi, S. Zein in Controlled Drug Delivery and Tissue Engineering. *J. Controlled Release* **2014**, *189*, 108−122.

(16) Di Martino, A.; Sittinger, M.; Risbud, M. V. Chitosan: A Versatile Biopolymer for Orthopaedic Tissue-Engineering. *Biomaterials* **2005**, *26* (30), 5983−5990.

(17) Kim, I.; Seo, S.; Moon, H.; Yoo, M.; Park, I.; Kim, B.; Cho, C. *Biotechnol. Adv.* **2008**, *26*, 1−21.

(18) Chew, S. L.; Wang, K.; Chai, S. P.; Goh, K. L. Elasticity, Thermal Stability and Bioactivity of Polyhedral Oligomeric Silsesquioxanes Reinforced Chitosan-Based Microfibres. *J. Mater. Sci.: Mater. Med.* **2011**, *22* (6), 1365−1374.

(19) Wu, C. J.; Gaharwar, A. K.; Schexnailder, P. J.; Schmidt, G. Development of Biomedical Polymer-Silicate Nanocomposites: A Materials Science Perspective. *Materials* **2010**, *3* (5), 2986−3005.

(20) Narayanan, K. B.; Sakthivel, N. Green Synthesis of Biogenic Metal Nanoparticles by Terrestrial and Aquatic Phototrophic and Heterotrophic Eukaryotes and Biocompatible Agents. *Adv. Colloid Interface Sci.* **2011**, *169* (2), 59−79.

(21) Madhumathi, K.; Sudheesh Kumar, P. T.; Kavya, K. C.; Furuike, T.; Tamura, H.; Nair, S. V.; Jayakumar, R. Novel Chitin/Nanosilica Composite Scaffolds for Bone Tissue Engineering Applications. *Int. J. Biol. Macromol.* **2009**, *45* (3), 289−292.

(22) Puchol, V.; El Haskouri, J.; Latorre, J.; Guillem, C.; Beltrán, A.; Beltrán, D.; Amorós, P. Biomimetic Chitosan-Mediated Synthesis in Heterogeneous Phase of Bulk and Mesoporous Silica Nanoparticles. *Chem. Commun.* **2009**, 2694−2696.

(23) Pietak, A. M.; Reid, J. W.; Stott, M. J.; Sayer, M. Silicon Substitution in the Calcium Phosphate Bioceramics. *Biomaterials* **2007**, *28* (28), 4023−4032.

(24) Bunpetch, V.; Zhang, X.; Li, T.; Lin, J.; Maswikiti, E. P.; Wu, Y.; Cai, D.; Li, J.; Zhang, S.; Wu, C.; et al. Silicate-Based Bioceramic Scaffolds for Dual-Lineage Regeneration of Osteochondral Defect. *Biomaterials* **2019**, *192*, 323−333.

(25) Ran, J.; Jiang, P.; Sun, G.; Ma, Z.; Hu, J.; Shen, X.; Tong, H. Comparisons among Mg, Zn, Sr, and Si Doped Nano-Hydroxyapatite/Chitosan Composites for Load-Bearing Bone Tissue Engineering Applications. *Mater. Chem. Front.* **2017**, *1* (5), 900−910.

(26) Deng, C.; Zhu, H.; Li, J.; Feng, C.; Yao, Q.; Wang, L.; Chang, J.; Wu, C. Bioactive Scaffolds for Regeneration of Cartilage and Subchondral Bone Interface. *Theranostics* **2018**, *8* (7), 1940−1955.

(27) Cho, J.; Joshi, M. S.; Sun, C. T. Effect of Inclusion Size on Mechanical Properties of Polymeric Composites with Micro and Nano Particles. *Compos. Sci. Technol.* **2006**, *66* (13), 1941−1952.

(28) Kannan, R. Y.; Salacinski, H. J.; Butler, P. E.; Seifalian, A. M. Polyhedral Oligomeric Silsesquioxane Nanocomposites: The Next Generation Material for Biomedical Applications. *Acc. Chem. Res.* **2005**, *38* (11), 879−884.

(29) Ghanbari, H.; Cousins, B. G.; Seifalian, A. M. A Nanocage for Nanomedicine: Polyhedral Oligomeric Silsesquioxane (POSS). *Macromol. Rapid Commun.* **2011**, *32* (14), 1032−1046.

(30) McCusker, C.; Carroll, J. B.; Rotello, V. M. Cationic Polyhedral Oligomeric Silsesquioxane (POSS) Units as Carriers for Drug Delivery Processes. *Chem. Commun.* **2005**, *1* (8), 996−998.

(31) Kannan, R. Y.; Salacinski, H. J.; Groot, J. De; Clatworthy, I.; Bozec, L.; Horton, M.; Butler, P. E.; Seifalian, A. M. The Antithrombogenic Potential of a Polyhedral Oligomeric. *Biomacromolecules* **2006**, *7*, 215−223.

(32) Knight, P. T.; Lee, K. M.; Qin, H.; Mather, P. T. Polyhedral Oligosilsesquioxane. *Biomacromolecules* **2008**, *9*, 2458−2467.

(33) Dodiuk-Kenig, H.; Maoz, Y.; Lizenboim, K.; Eppelbaum, I.; Zalsman, B.; Kenig, S. The Effect of Grafted Caged Silica (Polyhedral Oligomeric Silsesquioxanes) on the Properties of Dental Composites and Adhesives. *J. Adhes. Sci. Technol.* **2006**, *20* (12), 1401−1412.

(34) Kim, S. K.; Heo, S. J.; Koak, J. Y.; Lee, J. H.; Lee, Y. M.; Chung, D. J.; Lee, J. I.; Hong, S. D. A Biocompatibility Study of a Reinforced Acrylic-Based Hybrid Denture Composite Resin with Polyhedraloligosilsesquioxane. *J. Oral Rehabil.* **2007**, *34* (5), 389−395.

(35) Ha, Y. M.; Amna, T.; Kim, M. H.; Kim, H. C.; Hassan, S. S. M.; Khil, M. S. Novel Silicificated PVAc/POSS Composite Nanofibrous Mat via Facile Electrospinning Technique: Potential Scaffold for Hard Tissue Engineering. *Colloids Surf., B* **2013**, *102*, 795−802.

(36) Oseni, A. O.; Butler, P. E.; Seifalian, A. M. The Application of POSS Nanostructures in Cartilage Tissue Engineering: The Chondrocyte Response to Nanoscale Geometry. *J. Tissue Eng. Regener. Med.* **2015**, *9* (11), E27−E38.

(37) Rizk, M.; Hohlfeld, L.; Thanh, L. T.; Biehl, R.; Lühmann, N.; Mohn, D.; Wiegand, A. Bioactivity and Properties of a Dental Adhesive Functionalized with Polyhedral Oligomeric Silsesquioxanes (POSS) and Bioactive Glass. *Dent. Mater.* **2017**, *33* (9), 1056−1065.

(38) Freier, T.; Koh, H. S.; Kazazian, K.; Shoichet, M. S. Controlling Cell Adhesion and Degradation of Chitosan Films by N-Acetylation. *Biomaterials* **2005**, *26* (29), 5872−5878.

(39) Bose, S.; Roy, M.; Bandyopadhyay, A. Recent Advances in Bone Tissue Engineering Scaffolds. *Trends Biotechnol.* **2012**, *30* (10), 546−554.

(40) Chen, Q.; Roether, J. A.; Boccaccini, a. R. Tissue Engineering Scaffolds from Bioactive Glass and Composite Materials. *Top. Tissue Eng.* **2008**, *4* (6), 1−27.

(41) Murphy, C. M.; Haugh, M. G.; O'Brien, F. J. The Effect of Mean Pore Size on Cell Attachment, Proliferation and Migration in Collagen-Glycosaminoglycan Scaffolds for Bone Tissue Engineering. *Biomaterials* **2010**, *31* (3), 461−466.

(42) Costa-Pinto, A. R.; Reis, R. L.; Neves, N. M. Scaffolds Based Bone Tissue Engineering: The Role of Chitosan. *Tissue Eng., Part B* **2011**, *17* (5), 331−347.

(43) Zhao, Y.; Schiraldi, D. A. Thermal and Mechanical Properties of Polyhedral Oligomeric Silsesquioxane (POSS)/Polycarbonate Composites. *Polymer* **2005**, *46* (25), 11640−11647.

(44) Kim, B. S.; Mather, P. T. Morphology, Microstructure, and Rheology of Amphiphilic Telechelics Incorporating Polyhedral Oligosilsesquioxane. *Macromolecules* **2006**, *39* (26), 9253−9260.

(45) Sprio, S.; Tampieri, A.; Landi, E.; Sandri, M.; Martorana, S.; Celotti, G.; Logroscino, G. *Mater. Sci. Eng., C* **2008**, *28*, 179−187.

(46) Nakata, K.; Kubo, T.; Numako, C.; Onoki, T.; Nakahira, A. Synthesis and Characterization of Silicon-Doped Hydroxyapatite. *Mater. Trans.* **2009**, *50* (5), 1046−1049.

(47) Martínez-vázquez, F. J.; Cabañas, M. V.; Paris, J. L.; Lozano, D.; Vallet-regí, M. Fabrication of Novel Si-Doped Hydroxyapatite/Gelatine Scaffolds by Rapid Prototyping for Drug Delivery and Bone Regeneration. *Acta Biomater.* **2015**, *15*, 200−209.

(48) Sroka-Bartnicka, A.; Borkowski, L.; Ginalska, G.; Ślósarczyk, A.; Kazarian, S. G. Structural Transformation of Synthetic Hydroxyapatite under Simulated in Vivo Conditions Studied with ATR-FT-IR Spectroscopic Imaging. *Spectrochim. Acta, Part A* **2017**, *171*, 155−161.

(49) Tamburaci, S.; Tihminlioglu, F. Diatomite Reinforced Chitosan Composite Membrane as Potential Scaffold for Guided Bone Regeneration. *Mater. Sci. Eng., C* **2017**, *80*, 222−231.

(50) Torres-Giner, S.; Gimenez, E.; Lagaron, J. M. Characterization of the Morphology and Thermal Properties of Zein Prolamine Nanostructures Obtained by Electrospinning. *Food Hydrocolloids* **2008**, *22* (4), 601−614.

(51) Vogt, L.; Liverani, L.; Roether, J.; Boccaccini, A. Electrospun Zein Fibers Incorporating Poly (Glycerol Sebacate) for Soft Tissue Engineering. *Nanomaterials* **2018**, *8* (3), 150.

(52) Gianazza, E.; Viglienghi, V.; Righetti, P. G.; Salamini, F.; Soave, C. Amino Acid Composition of Zein Molecular Components. *Phytochemistry* **1977**, *16* (3), 315−317.

(53) Wu, S.; Qin, X.; Li, M. The Structure and Properties of Cellulose Acetate Materials: A Comparative Study on Electrospun Membranes and Casted Films. *J. Ind. Text.* **2014**, *44* (1), 85−98.

(54) Deng, L.; Kang, X.; Liu, Y.; Feng, F.; Zhang, H. Characterization of Gelatin/Zein Films Fabricated by Electrospinning vs Solvent Casting. *Food Hydrocolloids* **2018**, *74*, 324−332.

(55) Faucheux, N.; Schweiss, R.; Lützow, K.; Werner, C.; Groth, T. Self-Assembled Monolayers with Different Terminating Groups as Model Substrates for Cell Adhesion Studies. *Biomaterials* **2004**, *25* (14), 2721−2730.

(56) Tzoneva, R.; Faucheux, N.; Groth, T. Wettability of Substrata Controls Cell-Substrate and Cell-Cell Adhesions. *Biochim. Biophys. Acta, Gen. Subj.* **2007**, *1770* (11), 1538−1547.

(57) Yuan, Y.; Lee, T. R. Contact Angle and Wetting Properties. *Springer Ser. Surf. Sci.* **2013**, *51*, 3−34.

(58) Xianmiao, C.; Yubao, L.; Yi, Z.; Li, Z.; Jidong, L.; Huanan, W. Properties and in Vitro Biological Evaluation of Nano-Hydroxyapatite/Chitosan Membranes for Bone Guided Regeneration. *Mater. Sci. Eng., C* **2009**, *29* (1), 29−35.

(59) Pallela, R.; Venkatesan, J.; Janapala, V. R.; Kim, S. K. Biophysicochemical Evaluation of Chitosan-Hydroxyapatite-Marine Sponge Collagen Composite for Bone Tissue Engineering. *J. Biomed. Mater. Res., Part A* **2012**, *100A* (2), 486−495.

(60) Park, S. M.; Kim, H. S. Preparation of Acetylated Chitosan/Carbonated Hydroxyapatite Composite Barriers for Guided Bone Regeneration. *Macromol. Res.* **2017**, *25* (2), 158−164.

(61) Swetha, M.; Sahithi, K.; Moorthi, A.; Srinivasan, N.; Ramasamy, K.; Selvamurugan, N. Biocomposites Containing Natural Polymers and Hydroxyapatite for Bone Tissue Engineering. *Int. J. Biol. Macromol.* **2010**, *47* (1), 1−4.

(62) Sowjanya, J. A.; Singh, J.; Mohita, T.; Sarvanan, S.; Moorthi, A.; Srinivasan, N.; Selvamurugan, N. Biocomposite Scaffolds Containing Chitosan/Alginate/Nano-Silica for Bone Tissue Engineering. *Colloids Surf., B* **2013**, *109*, 294−300.

(63) Sionkowska, A.; Kaczmarek, B. Preparation and Characterization of Composites Based on the Blends of Collagen, Chitosan and Hyaluronic Acid with Nano-Hydroxyapatite. *Int. J. Biol. Macromol.* **2017**, *102*, 658−666.

(64) Dziadek, M.; Stodolak-Zych, E.; Cholewa-Kowalska, K. Biodegradable Ceramic-Polymer Composites for Biomedical Applications: A Review. *Mater. Sci. Eng., C* **2017**, *71*, 1175−1191.

(65) Marom, R.; Shur, I.; Solomon, R.; Benayahu, D. Characterization of Adhesion and Differentiation Markers of Osteogenic Marrow Stromal Cells. *J. Cell. Physiol.* **2005**, *202* (1), 41−48.

(66) Stucki, U.; Schmid, J.; Hämmerle, C. F.; Lang, N. P. Temporal and Local Appearance of Alkaline Phosphatase Activity in Early Stages of Guided Bone Regeneration. A Descriptive Histochemical Study in Humans. *Clin. Oral Implants Res.* **2001**, *12* (2), 121−127.

(67) Kavya, K. C.; Jayakumar, R.; Nair, S.; Chennazhi, K. P. International Journal of Biological Macromolecules Fabrication and Characterization of Chitosan/Gelatin/n SiO 2 Composite Scaffold for Bone Tissue Engineering. *Int. J. Biol. Macromol.* **2013**, *59*, 255−263.

(68) Gomez-Sanchez, C.; Kowalczyk, T.; Ruiz De Eguino, G.; Lopez-Arraiza, A.; Infante, A.; Rodriguez, C. I.; Kowalewski, T. A.; Sarrionandia, M.; Aurrekoetxea, J. Electrospinning of Poly(Lactic Acid)/Polyhedral Oligomeric Silsesquioxane Nanocomposites and Their Potential in Chondrogenic Tissue Regeneration. *J. Biomater. Sci., Polym. Ed.* **2014**, *25* (8), 802−825.

(69) Guasti, L.; Vagaska, B.; Bulstrode, N. W.; Seifalian, A. M.; Ferretti, P. Chondrogenic Differentiation of Adipose Tissue-Derived Stem Cells within Nanocaged POSS-PCU Scaffolds: A New Tool for Nanomedicine. *Nanomedicine* **2014**, *10* (2), 279−289.

(70) Hu, J. C. Y.; Athanasiou, K. A. Structure and Function of Articular Cartilage. *Handbook of Histology Methods for Bone and Cartilage*; Humana Press: Totowa, NJ, 2003; pp 73−95.